science, engineering and health studies

Research Article

Science, Engineering and Health Studies
https://lio1.tci-thaijo.org/index.php/sehs
ISSN (Online): 2630-0087

Walking pattern analysis using the gait cycle to classify a healthy and an unhealthy form

*Piyapon Suntikan and Wisan Tangwongcharoen**

Department of Computer Science, School of Science, King Mongkut's Institute of Technology Ladkrabang, Bangkok 10520, Thailand

ABSTRACT

This study proposed an algorithm to classify normal and abnormal forms of walking patterns by identifying the swing and stance phases, known as the gait cycle. The walking patterns were examined by collecting data using Razor IMU sensors. The Wi-Fi transmitter was utilized to transfer raw data for further analysis, representing the gait cycle using a linear graph. The data were preprocessed and transformed into phase graphs using the polar coordinate equation. To identify areas of density, data were incorporated into K-mean clustering. A k-value of 2 groups represented the major walking phases and classified patterns based on a regional model. The experimental results enable us to define healthy and unhealthy forms. This algorithm conveniently assists in diagnosing basic physical conditions, and the dataset is efficient for monitoring the medical treatment process among recipients.

Keywords: gait cycle; walking; fast Fourier transform; polar coordinate; K-mean clustering

***Corresponding author**:
Wisan Tangwongcharoen
wisan.ta@kmitl.ac.th

Received: *10 March 2023*
Revised: *15 October 2023*
Accepted: *17 October 2023*
Published: *31 December 2023*

Citation:
Suntikan, P., and Tangwongcharoen, W. (2023). Walking pattern analysis by using gait cycle to classify a healthy and an unhealthy form. Science, Engineering and Health Studies, 17, 23040012.

1. INTRODUCTION

Healthcare trends are increasing in both the working-age and retirement-age populations. Modernization and innovative technologies contribute to extended life expectancy and reduce degeneration. In the realm of healthcare, food is no longer the sole concern; developing a workout habit is also considered an important step in addressing health problems. Those aiming to maintain good health often engage in regular exercise. Nowadays, there are many alternative activities available, with no-equipment workouts like fast walking and running as basic starters for everyone. Medical studies have shown that walking can reduce the risk of non-communicable diseases, diabetes, cancer, and osteoporosis. A daily walk can diminish excess fat (Campellone et al., 2023; Victory State Government, 2022). Although walking is a low-impact activity and has a low risk of injury, improper performance of body parts can lead to movement-related injuries. Walking involves the use of the hip, knee, and ankle. The continuous movement supporting each part is referred to the "gait cycle". The gait cycle is the cycle of walking comprising separated stages of leg movement. The major parts of walking have 2 stages: swing and stance (Soangra et al., 2022; Yakimovich et al., 2006; Romtrairat et al., 2020; Kongkhiaw, 2010). Assuming issues arise in these two parts are problematic, the walking pattern in each state will differ.

In the previous research paper (Kongkhiaw, 2010), the major walking pattern was defined using K-mean clustering to indicate healthy and unhealthy patterns for further prediction. However, we encountered challenges in calculating the angles within the abnormal range. Consequently, the raw walking data were processed using the fast Fourier transform, as a standard model for preprocessing wave data. This algorithm effectively reduced noise and recorded lost data. Following data preprocessing, the data were transformed into phase graphs using polar coordinates. At this stage, it showed the walking angle, the distribution of datapoints, and also the data

density. The final step in processing the graph would identify the density areas, presenting unusual data points indicative of irregular movement.

2. MATERIALS AND METHODS

2.1 Sensor and equipments

The Sparkfun 9-degree Razor IMU motion sensor was utilized in this study. The sensor components included a three-axis sensor with a gyroscope, accelerometer and magnetometer. Data were transmitted to the computer via ESP8266 Wi-Fi transmitter. Kinesio tape, or k-tape, was used to control muscles and reduce injuries in sports players. This tape is widely used in physical therapy and sport science, attaching sensors that enclose a body part in a specific position. The sensors are shown in Figure 1(a), and the k-tape is shown in Figure 1(b).

2.2 Gait cycle

Walking is an alternating rhythmic leg movement pattern that propels the body forward. The "gait cycle" represents the standard pattern for walking analysis. This cycle is composed of two major phases: the stance phase and the swing phase. The stance phase occurs when the foot is on the ground, providing support for leg movement, while the swing phase enables the foot to move forward freely without contacting the ground. During walking, both legs transition between these two phases with the support of all body parts. Consequently, any issues with specific body parts impact the walk formation. Abnormal walking can result from various problems, such as injury-related pain, muscle weakness, or restrictions in joint motion. These factors are analyzed to diagnose walking symptoms. The gait cycle and stages of movement (Kongkhiaw, 2010; Santikan et al., 2022; Inman et al., 1981) are depicted in Figure 2.

(a) (b)

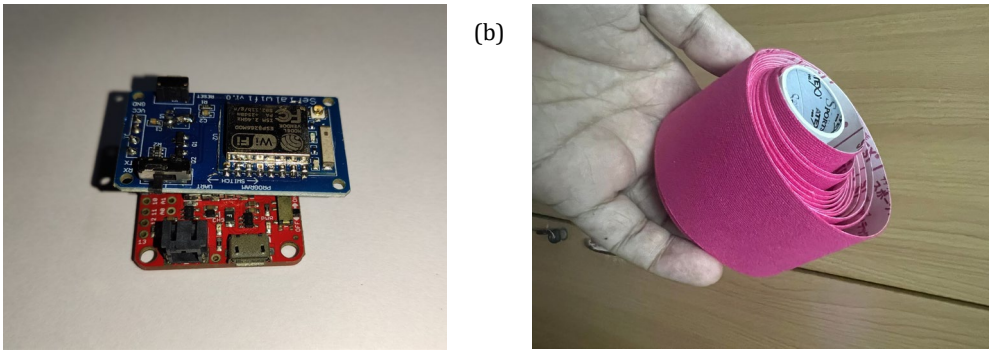

Figure 1. The equipment for gathering data: (a) Razor IMU and Wi-Fi, (b) k-tape

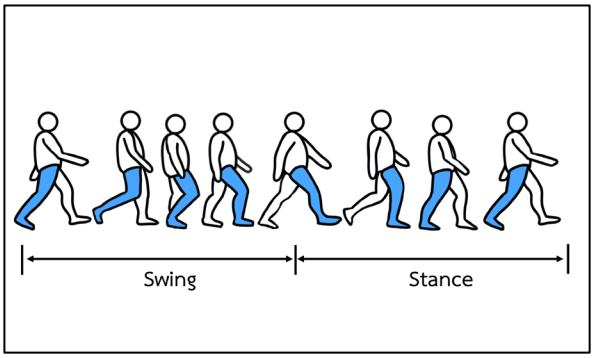

Figure 2. Gait Cycle

2.3 Rotation metrix

The rotation matrix controls the direction of the swivel, occurring in three dimensions along the longitudinal, vertical, and lateral axes. This theory is widely used in aircraft, sensors, and the robotics industry, involving rotations along the x, y, and z axes. All axis movements are related to each other (Rodgers, 1995; Seyrafi, 2009). The Razor IMU is constructed using a rotation matrix and gathers tilting along the x, y, and z axes. The relation of tilting is shown in Figure 3.

2.4 Fast Fourier transform (FFT)

The FFT is a mathematical methodology that transforms the time domain signal into the frequency domain (Johnson and Frigo, 2007). Rediscovered and published in 1965 by James Cooley and John Turkey, this algorithm provides a faster and more efficient method for computing the Fourier transform of a signal. It operates at O (N log(n)) scaling, in contrast to the, O(N2) scaling of discrete Fourier transform. Due to its strength, the FFT is widely implemented across various industries, such as radio and space, to reduce noise and outliers in signals. Its results not only produce a cleaner wave but also precise and higher-quality data due to the characteristics of the raw wave data. The FFT algorithm was used for preprocessing, as shown in Figure 4.

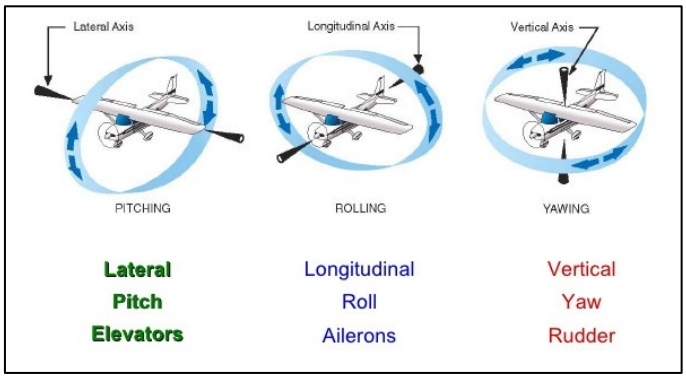

Figure 3. Naming of axes and direction of rotation (Microtronic, 2017)

```
algorithm iterative-fft is
  input: Array a of n complex values where n is a power of 2.
  output: Array A the DFT of a.

  bit-reverse-copy(a,A)
  n ← a.length
  for s = 1 to log(n) do
    m ← 2^s
    ωm ← exp(−2πi/m)
    for k = 0 to n-1 by m do
      ω ← 1
      for j = 0 to m/2 – 1 do
        t ← ω A[k + j + m/2]
        u ← A[k + j]
        A[k + j] ← u + t
        A[k + j + m/2] ← u – t
        ω ← ω ωm

  return A

algorithm bit-reverse-copy(a,A) is
  input: Array a of n complex values where n is a power of 2.
  output: Array A of size n.

  n ← a.length
  for k = 0 to n – 1 do
    A[rev(k)] := a[k]
```

Figure 4. Pseudocode of FFT (Johnson and Frigo, 2007)

2.5 Polar coordinate

In mathematical terms, the graph is outlined using the Cartesian system to plot x and y (Boyer, 1949). However, the Cartesian system is transformed into an angle through polar coordinates. Each point in the Cartesian plane is converted to a polar coordinate, considering both the distance and the angle from the original point. The angle within the polar coordinates ranges from 0 to 270 degrees, some of which are derived from radians. This calculation system is applied in boat sailing and area exploration. The relationship between the Cartesian system and polar coordinates involves converting the radius and angle to x and y using trigonometric functions. The relationship between Cartesian and polar coordinates is derived in Equations (1) and (2).

$$x = r\cos\theta \quad (1)$$

$$y = r\sin\theta \quad (2)$$

where r is the radius, $\boldsymbol{\theta}$ is the angle, x is the data on the x-axis, and y is the data on the y-axis.

2.6 K-mean clustering

The K-mean clustering algorithm is popular due to its utilization of uncomplicated variables for setup. Researchers have the option to select the number of clusters, k, by calculating the silhouette coefficient or by choosing a random k in the initial clustering round. For our research, centroids were initially established based on the angle of walking performance. The data groups were then clustered according to the distance from these centroids. In each round, new centroids were calculated until data convergence was achieved (Pelleg and Moore, 1999; Cormen et al., 2004; Hartigan and Wong, 1979). K-mean clustering was implemented as shown in Equation (3).

$$SSE = \sum_{i=1}^{2} \sum_{P \in c_i} dist\ (C_i, D_{i\ldots n})^2 \quad (3)$$

where i is the order of the data, C_i is the centroid of the cluster order i, and $D_{i\ldots n}$ are the average data of the testers.

To calibrate the mean for each round, Equation (4) is used.

$$C_i = \frac{1}{c_i}(D_1 + \ldots + D_n) \quad (4)$$

where C_i is the centroid of the cluster order i, c_i is the average data of the testers, and D_n is the number of points in the Euler graphs.

2.7 Methodology

This section outlines the research algorithm with seven steps, as depicted in Figure 5.

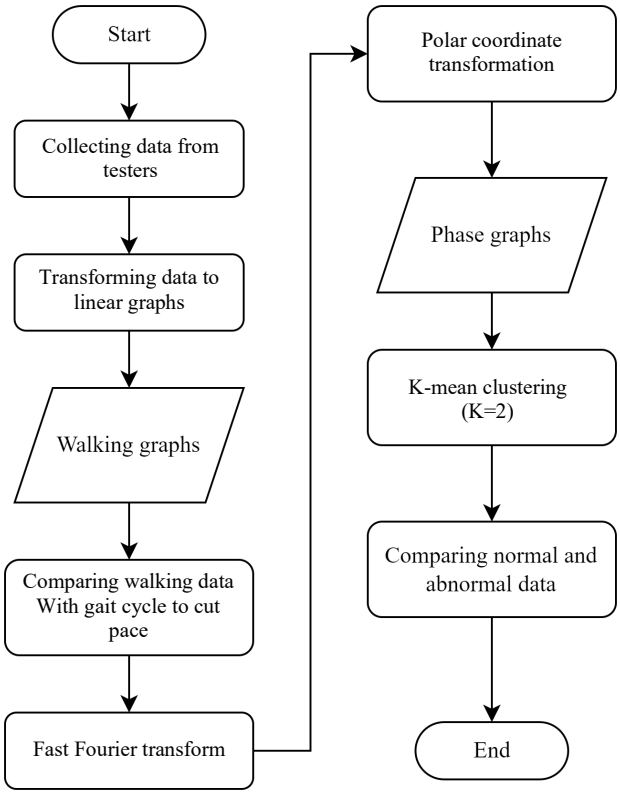

Figure 5. Research methodology

Seven sensors were attached to the main body parts: the hips, knees, and ankles. After preparing the equipment, the tester walked a 4-meter round-trip. Once the collection process was completed, the raw walking data were transformed into a linear graph. This stage was compared with the gait cycle to extract pace data. Additionally, the walking phase was compared with linear graphs to be analyzed in the next step. The generated pace data underwent preprocessing using the fast Fourier transform, resulting in the creation of phase graph data in this step. The data files were saved as the Excel files. The pace in the phase graphs was categorized through the K-mean algorithm, where k=2 was chosen to describe the major walking phases. K-means clustering categorized the density of the data and created the density area, specifying both normal and abnormal patterns.

2.8 Collecting walking data using Razor IMU

We collaborated with Rangsit University to conduct tests on approximately 30 cases, involving both normal and abnormal testers. The testing process was designed by a physiotherapist. Prior to the walking test, seven sensors were affixed on various body parts using k-tape. During the walking test, the movement showed a correlation between the hips, knees, and ankles, aligning with the walking theory. The method of attaching sensors is illustrated in Figure 6.

Figure 6. The position of Razor IMU

2.9 Linear graphs to clarify the gait cycle

This section details the application of a linear graph related to the major walking phases for identifying symptoms of walking patterns. It observes the variation in data between normal and abnormal phases. This was achieved by segmented the long sine wave, representing raw data, into smaller pace and indicating the walking phase, as shown in Figure 7.

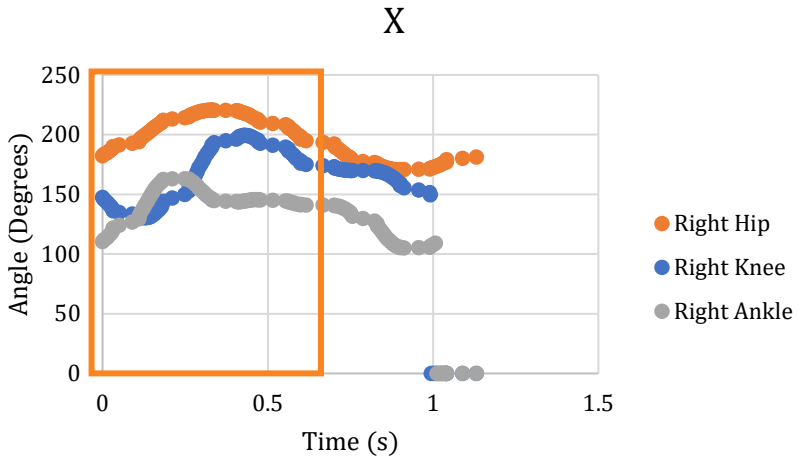

Figure 7. Linear graphs

2.10 Reducing noise and tuning the data with FFT

This step was executed using Python programming with the FFT function in order to generate data. Each data item of one pace was processed through an Excel file, and variables were set up to tune the data. The data transformation via the FFT generated a threshold value to indicate frequency-based noise. After computation, the noise was removed to ensure data integrity. The FFT function is depicted in Figure 8.

3. RESULTS

The data from test subjects were transformed into a linear graph representing data behavior. Once the knee joint movement data behavior was understood, grouping and classification were performed using the K-mean clustering and coefficients. The classification aimed to distinguish between healthy and unhealthy patterns, with the optimal value of k calculated to establish these pattern results. The results were collected from 30 test subjects with both healthy and unhealthy knees.

3.1 Linear graphs results

Each test subject's gait was transformed into linear graphs to compare with the gait cycle. The objective was to define the walking phase and segment the entire walking dataset into only one pace, indicating the swing and stance phases distinctly. The angles in x, y, and z between times were measured to assess the performance of the hips, knees, and ankles within a single pace. The healthy pattern linear graphs on each axis are shown in Figure 9, and the unhealthy pattern linear graphs on each axis are shown in Figure 10.

```
fft_process(f_original_data, time_series, threshold):
    ## Compute the Fast Fourier Transform (FFT)
    n = lenght(time_series)
    f_hat = fft(original_data,time_series)  # Compute the FFT
    PSD = fhat * conjugate(f_hat) / n    # Power spectrum (power per freq)

    ## Use the PSD to filter out noise

    indices = PSD > threshold # Find all freqs with large power
    PSDclean = PSD * indices  # Zero out all others
    f_hat = indices * f_hat     # Zero out small Fourier coeffs. in Y
    f_filtered = ifft(f_hat) # Inverse FFT for filtered time signal

    return f_filtered

#Threshold specify
hip_pitch_fft = fft_process(hip_pitch, hip_time, 1000)
knee_pitch_fft = fft_process(knee_pitch, knee_time, 1000)
ankle_pitch_fft = fft_process(ankle_pitch, ankle_time, 100)

hip_roll_fft = fft_process(hip_roll, hip_time, 100)
knee_roll_fft = fft_process(knee_roll, knee_time, 100)
ankle_roll_fft = fft_process(ankle_roll, ankle_time, 100)

hip_yaw_fft = fft_process(hip_yaw, hip_time, 100)
knee_yaw_fft = fft_process(knee_yaw, knee_time, 100)
ankle_yaw_fft = fft_process(ankle_yaw, ankle_time, 100)
```

Figure 8. FFT function set up in python programing

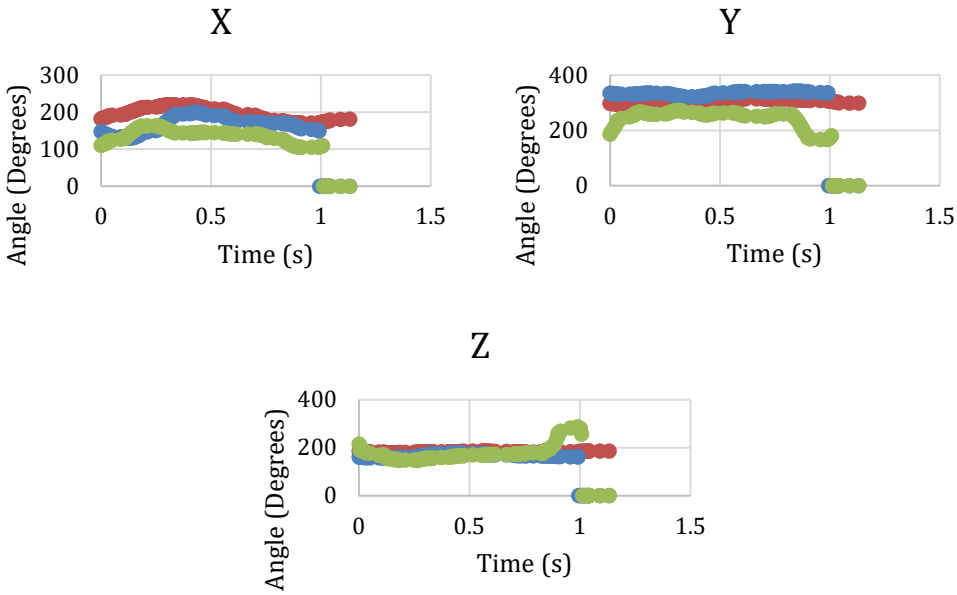

Figure 9. Linear graph of the healthy test subjects

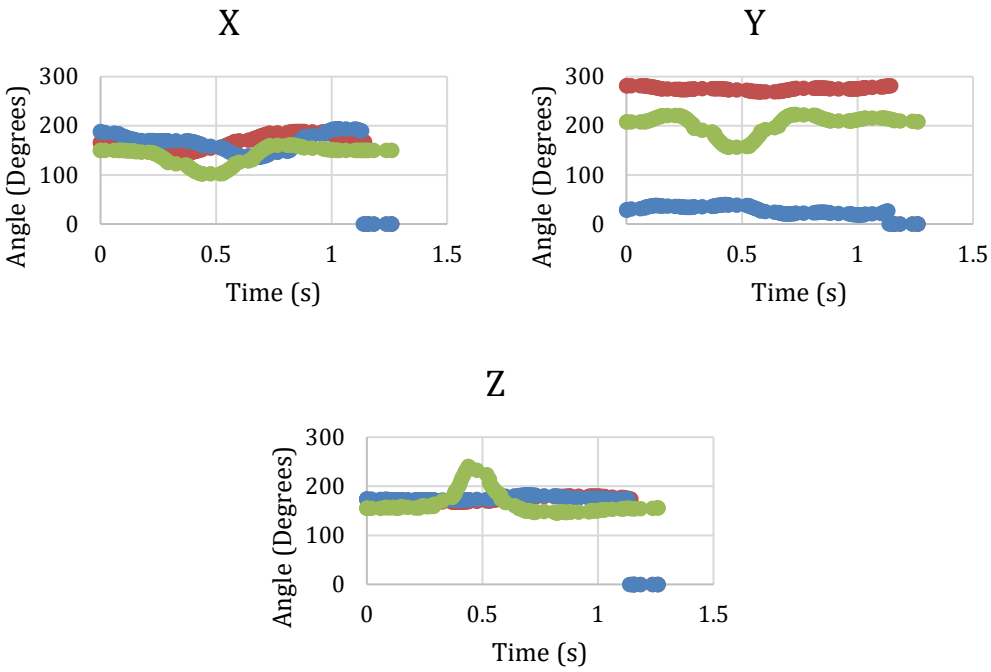

Figure 10. Linear graph of the unhealthy test subjects

In a typical x-axis pattern, the hips moved within an angle range of approximately 200–250 degrees. Initially, they angled down near the ground, reaching almost 210 degrees as the knee angles upwards. Along the y-axis, the hips and shins maintained similar angles, while the ankles maintained an approximately 200-degree angle until the completion of the swing phase. Notably, in the z-axis, minimal variation was observed as the displacement plane remained relatively unchanged in that direction. In atypical x-axis patterns, the hips deviated below 200 degrees and rose significantly during a full stride. The shins angled downward, reaching approximately 150 degrees towards the end of the stance phase, while the knee joint quickly rebounds. In addition, the shins closely align with the x-axis, contrasting with the torsion observed in the z-axis of the ankles. These movements result in a rise to 250 degrees in the z-axis within the graph.

3.2 Phase graph results

Healthy pattern results are shown in Figure 11. The results of the unhealthy pattern demonstrated characteristic movement patterns observed in individuals with health issues. The data showcasing movement angles in 3 dimensions for each body part is presented, and the comparison of the movement angles in each axis is shown in Figure 12.

The advantage of phase pattern graphing lies in its ability to clarify the data density. Our hypothesis suggested that individuals with abnormal patterns exhibited higher density, compared to normal individuals. This hypothesis was based on the abnormal frequency and quicker movement, attributed to their inability to directly bear weight on certain organs.

3.3 K-mean clustering results

This section shows experimental results concerning the clustering area. These areas provided insights into the incline parts of the data, indicating specific problematic areas within the unhealthy form. During this stage, we implemented k=2 to distinguish the swing and stance phases. When segmenting the data into individual paces, the reduced dataset size aligned well with the optimal value of k=2 for these datasets. Importantly, the color of each cluster did not signify the swing or stance phase; instead, it was used to visually represent the boundary of the areas. Moreover, the color corresponded to the density of data within each respective cluster. The healthy pattern results are shown in Figure 13, and the unhealthy pattern results are shown in Figure 14.

In the hip movement data of normal people along the x-axis, Group 1 had an area equivalent to Group 2. In contrast, for abnormal people, Group 2 had a larger area than Group 1 along the y-axis, being denser than the first group. Abnormal individuals showed similar areas. In the z-axis, both normal and abnormal data demonstrated similarities.

For knee movement data in the x-axis for normal individuals, Group 1 exhibited a larger area than Group 2. Conversely, for abnormal people, Group 2 had a larger area than Group 1 along the y-axis. The two areas were evenly divided. In the z-axis, normal individuals had similar areas for both Group 1 and Group 2, while abnormal individuals in Group 2 had more extensive areas than Group 1.

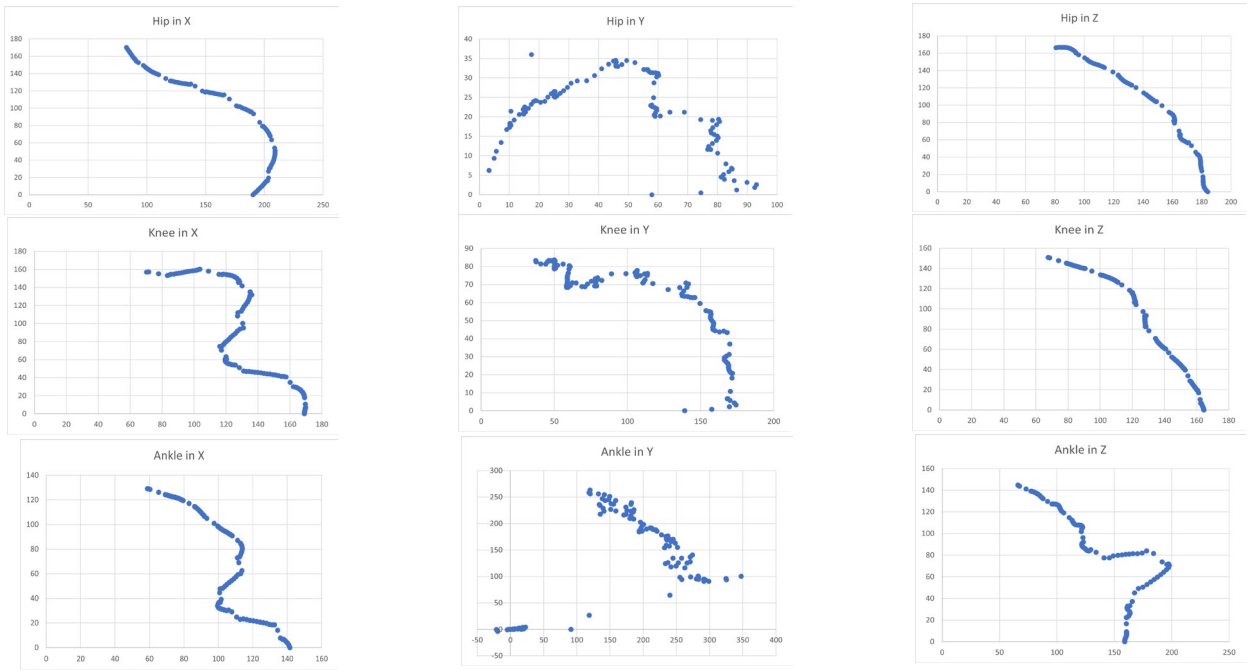

Figure 11. Healthy pattern: (a) data in the x, (b) data in the y, and (c) data in the z

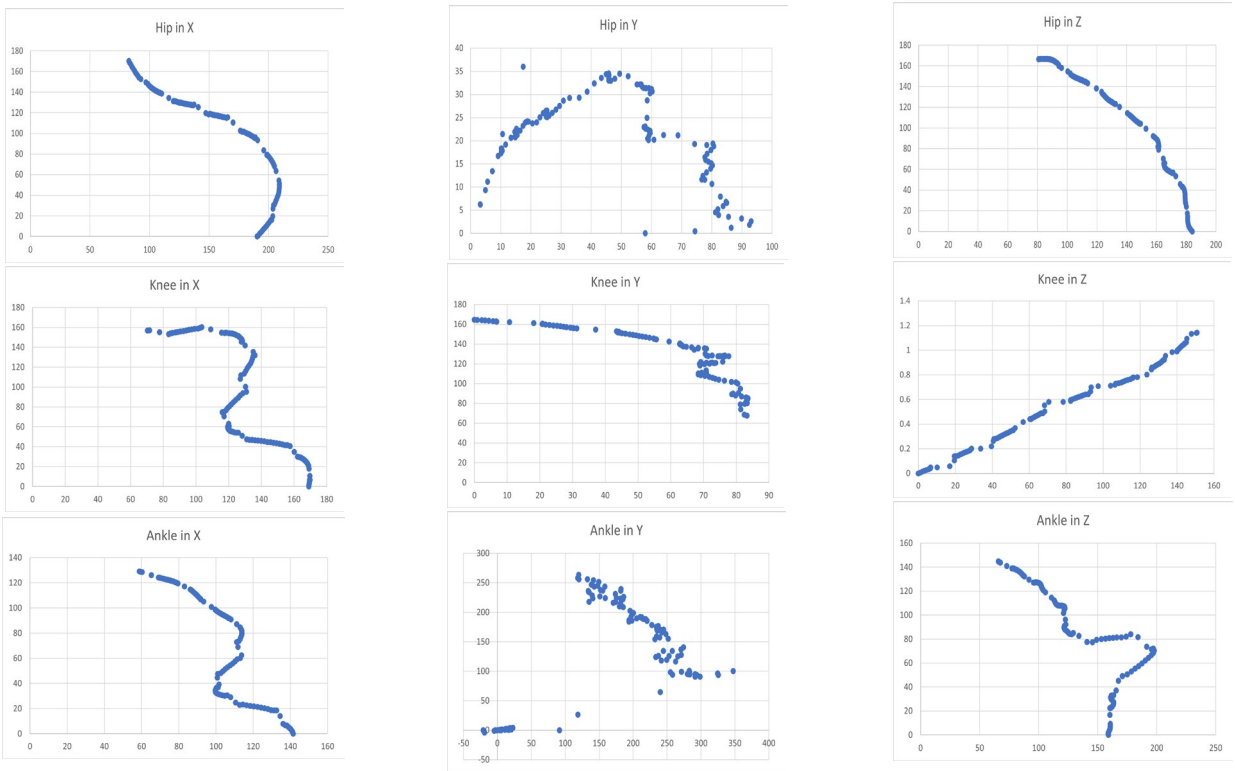

Figure 12. Unhealthy pattern: (a) data in the x, (b) data in the y, and (c) data in the z

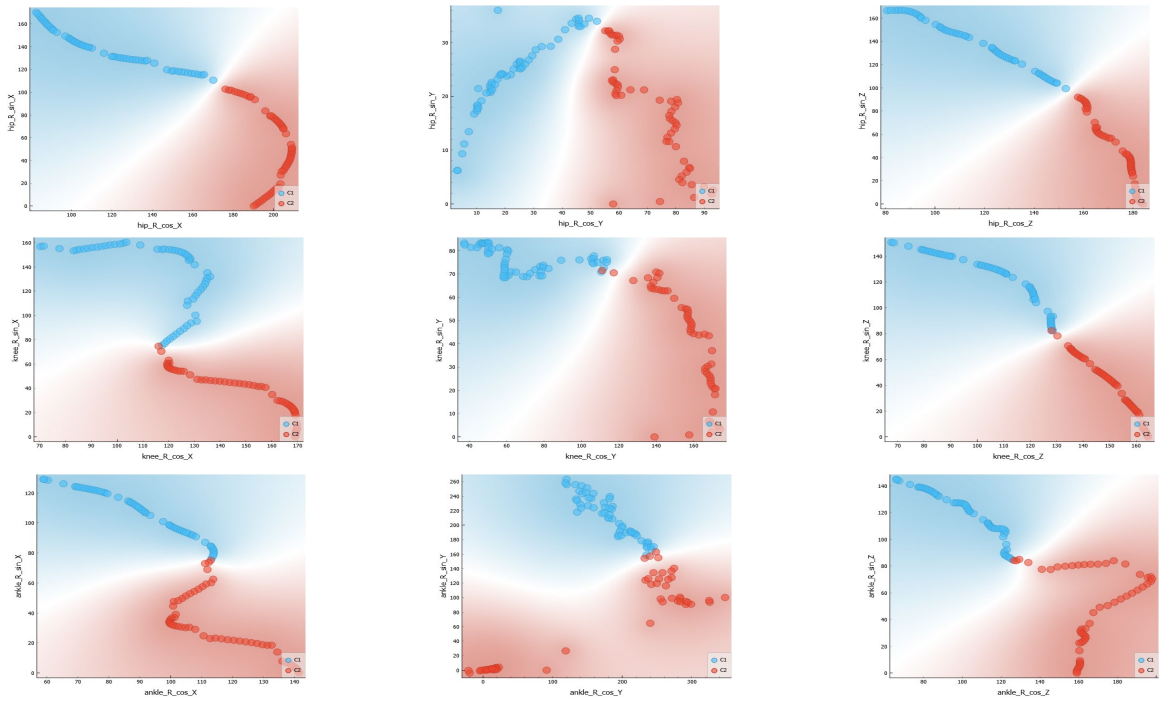

(a) (b) (c)

Figure 13. Healthy pattern clustering area: (a) data in the pitch axis, (b) data in the yaw axis, and (c) data in the roll axis

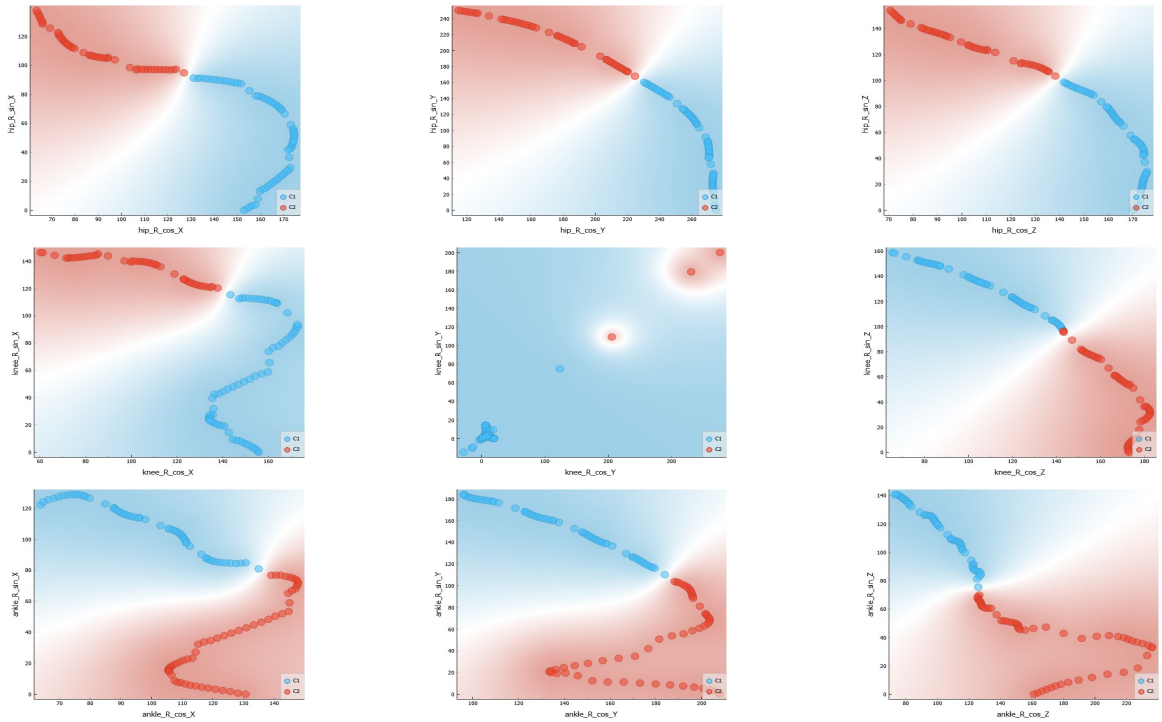

(a) (b) (c)

Figure 14. Unhealthy pattern clustering area: (a) data in the pitch axis, (b) data in the yaw axis, and (c) data in the roll axis

In the x-axis ankle movement data of normal people, Group 1 had a smaller area, compared to Group 2. Conversely, for abnormal people, Group 1 had a larger area than Group 2 along the y-axis. Additionally, Group 2 had an equivalent area share. Abnormal data in the second group were denser than the first group across the entire area. In the z-axis, normal individuals showed similar areas for both Group 1 and Group 2, while abnormal individuals in Group 2 had more extensive areas than Group 1.

The K-mean grouping allowed for a clear distinction between normal and abnormal walking patterns, revealing the distorted movements of abnormal individuals and facilitating an in-depth analysis of each organ part's movement. Identification of abnormal organs was possible through the analysis of data in this format. The regional classification was utilized to discern patterns. In normal hip movement, the upper part of the yaw axis had smaller areas compared to the abnormal movement. In normal knee movement, the upper areas of the pitch and yaw axes had a greater area than the abnormal. For the normal ankle movement area, the lower area is bigger than that of the abnormal movement.

4. DISCUSSION

In this study, seven sensors were attached to the main body parts—hips, knees, and ankles—to capture the complete gait cycle. Previous studies have employed the IMU sensor for movement detection (Tadano et al., 2016; Yuan and Chen, 2014; Tadano et al, 2013; Anwary et al., 2018), with a focus on refining sensor connectivity. In addition, the papers investigated gait pattern for both the right and left legs to enhance walking (Anwary et al., 2018; Chattopadhyay and Nandy, 2018; Romtrairat et al., 2020). Subsequently, the model was trained to validate the hypothesis and define the walking patterns. However, the use of multiple sensors required careful consideration of data connectivity. Some researchers preferred using only three sensors to minimize data loss and maintain data quality. Therefore, our work involved optimizing both the network and sensor connections. This approach not only enabled us to capture more detailed movement information but also avoided technical issues, resulting in smoother and higher-quality data. After the gait cycle data were retrieved, it was possible to define density areas of walking based on standard formations. This enabled the calculation of area differences, showing the areas affecting movement. Such analysis supports physical therapists and doctors in tracking the improvements in medical treatments and analyzing basic symptoms in certain cases.

5. CONCLUSION

This research focused on studying the gait cycle to distinguish between normal and abnormal walking patterns by proposing an algorithm to identify the cause of walking issues. Specially designed equipment was employed to collect data and apply the algorithm to identify the pattern of each part. The raw data were presented in linear graphs, serving as a reliable reference for the gait cycle. Detailed data distribution was achieved by focusing on a single pace during extended walks. The pace data underwent processing through the FFT algorithm to rectify the data loss and remove noise. After the algorithm processing, the pace data were transformed into a phase graph using polar coordinates equations. When the density was visualized, K-mean clustering was used to indicate the area of the density group, enabling the identification of problematic body areas. Consequently, the proposed algorithm within the equipment can assist doctors in diagnosing walking problems more effectively.

REFERENCES

Anwary, A. R., Yu, H., and Vassallo, M. (2018). Optimal foot location for placing wearable IMU sensors and automatic feature extraction for gait analysis. *IEEE Sensors Journal*, 18(6), 2555–2567.

Boyer, C. B. (1949). Newton as an originator of polar coordinates. *American Mathematical Monthly*, 56(2), 73–78.

Campellone, J. V., Dugdale, D. C., and Conaway, B. (2023). Walking abnormalities. Mount Sinai. [Online URL: https://www.mountsinai.org/health-library/symptoms/walking-abnormalities] accessed on October 19, 2023.

Chattopadhyay, S., and Nandy, A. (2018). Human gait modeling using hidden Markov model for abnormality detection. In *TENCON 2018 – 2018 IEEE Region 10 Conference*, Jeju, Korea (South). October 28-31.

Cormen, H. T., Leiserson, C. E., and Rivest R. L., and Stein, C., (2004). *Introduction to Algorithms*, 3rd, Cambridge: The MIT Press, pp. 915–918.

Hartigan, J. A., and Wong, M. A. (1979). Algorithm AS 136: A k-means clustering algorithm. *Journal of the Royal Statistical Society*. *Series C (Applied Statistics)*, 28(1), 100–108.

Inman, V. T., Ralston, H. J., and Todd, F. (1981). *Human Walking,* Baltimore: Williams and Wilkins, pp. 154-156.

Johnson, S. G., and Frigo, M. (2007). A modified split-radix FFT with fewer arithmetic operations. *IEEE Transactions on Signal Processing*, 55(1), 111–119.

Kongkhiaw, C. (2010). *Video system for dynamic motion analysis of human gait.* Master's thesis. Prince of Songkhla University, Thailand.

Microtronic. (2017). Roll, Pitch, Yaw. [Online URL: https://4.bp.blogspot.com/-ke68uluPCc/WPyIpowu9jI/AAAAAAAADuE/EqAOFzyqYKAr6QtI1A7T8z7dOFFipyc9wCLcB/s640/advanced-aerodynamics-4-728.jpg] accessed on October 19, 2023. [in Thai]

Pelleg, D., and Moore, A. (1999). Accelerating exact *k*-means algorithms with geometric reasoning. In *Proceedings of the Fifth ACM SIGKDD International Conference on Knowledge Discovery and Data Mining,* pp. 277–281. California, USA.

Rodgers, M. M. (1995). Dynamic foot biomechanics. *Journal of Orthopaedic and Sports Physical Therapy*, 21(6), 306–316.

Romtrairat, P., Virulsri, C., Wattanasiri, P., and Tangpornprasert, P. (2020). A performance study of a wearable balance assistance device consisting of scissored-pair control moment gyroscopes and a two-axis inclination sensor. *Journal of Biomechanics*, 109, 109957.

Santikan, P., Tangwongcharoen, W., and Kimpan, W. (2022). Define stance and swing pattern of gait cycle using motion sensor and k-mean clustering. In *Proceeding of the 19th International Conference on Electrical*

Engineering/Electronics Computer, Telecommunications and Information Technology (ECTI-CON), pp. 1–4. Prachuap Khiri Khan, Thailand.

Seyrafi, A. (2009). *Real time automatic step detection in the three dimensional accelerometer signal implemented on a microcontroller system*. Master's thesis. Blekinge Institute of Technology, Sweden.

Soangra, R., Wen, Y., Yang, H., and Grant-Beuttler, M. (2022). Classifying toe walking gait patterns among children diagnosed with idiopathic toe walking using wearable sensors and machine learning algorithms. *IEEE Access*, 10, 77054–77067.

Tadano, S., Takeda, R., and Miyagawa, H. (2013). Three dimensional gait analysis using wearable acceleration and gyro sensors based on quaternion calculations. *Sensors*, 13(7), 9321–9343.

Tadano, S., Takeda, R., Sasaki, K., Fujisawa, T., and Tohyama, H. (2016). Gait characterization for osteoarthritis patients using wearable gait sensors (H-Gait systems). *Journal of Biomechanics*, 49(5), 684–690.

Victory State Government. (2022). *Walking for good health*. Better Health Channel. [Online URL: https://www.betterhealth.vic.gov.au/health/healthyliving/walking-for-good-health] accessed on October 19, 2023.

Yakimovich, T., Kofman, J., and Lemaire, E. D. (2006). Design and evaluation of a stance-control knee-ankle-foot orthosis knee joint. *IEEE Transactions on Neural Systems and Rehabilitation Engineering*, 14(3), 361–369.

Yuan, Q., and Chen, I.-M. (2014). Localization and velocity tracking of human via 3 IMU sensors. *Sensors and Actuators A: Physical*, 212, 25–33.